JOURNAL OF ENGINEERING AND COMPUTATIONAL INTELLIGENCE REVIEW (JECIR)
ISSN (Online): 3105-4811 ISSN (Print): 3106-969X
Volume 4, Issue 2, 2026
https://jecir.com/

INVESTIGATING THE KINETICS OF Cu^{2+}-CATALYZED OXIDATION OF ASCORBIC ACID ($C_6H_8O_6$) IN AQUEOUS SOLUTIONS

Shah Wali Ullah [1], Zaid Ullah [2]

Affiliations

[1] Advanced Functional Materials (AFM) Laboratory, Engineering Physics Department, Institute Technology Bandung, Indonesia
33323751@mahasiswa.itb.ac.id

[2] Department of Chemistry, Islamia College Peshawar, Pakistan
zaid@icp.edu.pk

Corresponding Author's Email

[1] 33323751@mahasiswa.itb.ac.id

ABSTRACT

Ascorbic acid degrades rapidly in aerated aqueous media through catalysis by trace Cu^{2+}, yet published rate constants remain fragmented across dissimilar conditions and complete activation parameters are unavailable. This study establishes an internally consistent kinetic description of this reaction. Progress was followed spectrophotometrically at 265 nm under pseudo-first-order conditions while ascorbic acid (2.0–12.0 × 10^{-5} mol L^{-1}), Cu^{2+} (4.0 × 10^{-6}–1.0 × 10^{-4} mol L^{-1}), pH (3.0–6.0), ionic strength (0.01–0.50 mol L^{-1} KNO_3) and temperature (288–318 K) were varied systematically. The reaction was first order in both substrate and catalyst, giving k_{cat} = 277 ± 8 L mol^{-1} s^{-1} at 298 K, pH 4.5 and I = 0.10 mol L^{-1}. The ascorbate monoanion was forty times more reactive than the neutral diacid, and a negative Brønsted–Bjerrum slope confirmed oppositely charged reactants in the rate-determining step. Normalising for dissolved oxygen raised the activation energy from 38.8 to 52.0 kJ mol^{-1}, with $\Delta S‡$ = −76.4 J mol^{-1} K^{-1}, indicating an associative inner-sphere pathway.

Keywords: Ascorbic Acid; Vitamin C; Copper(II); Homogeneous Catalysis; Chemical Kinetics; Rate Law; Activation Energy; Autoxidation; UV-VIS Spectrophotometry

I. INTRODUCTION

L-Ascorbic acid ($C_6H_8O_6$) is a biologically important, pharmaceutical, nutritional and industrial water soluble micronutrient of great importance. The antioxidant activity is correlated with the presence of the C2–C3 ene-diol structure which is easily donating electrons and the radical ascorbate structure is prone to oxidation to dehydroascorbic acid. This redox activity is useful for ascorbic acid to neutralize the reactive oxygen species and prevent the damage to the cellular components. In the case of transition metals, however, the same compound can behave as a pro-oxidant, increasing the formation of radicals and oxidative reactions [1]. This dual chemical function has received much interest in the field of biomedical research, especially for studies investigating the potential application of high dose ascorbic acid in cancer therapy, where the effect of the ascorbic acid is highly dependent upon concentration, metal availability, and the redox environment [2]. Furthermore, ascorbic acid is used in the food industry for many purposes, as a pharmaceutical agent, and in cosmetic products owing to its antioxidant and reducing properties.

However, ascorbic acid is not a very stable chemical, especially in an aqueous and oxygen-rich environment, and thus it has limited uses. It is easily broken down by heat, oxygen, light, pH changes and catalyst-contaminating impurities, thus decreasing its nutritional value and functional efficacy. Kinetic studies have demonstrated that reaction rate of ascorbic acid degradation is strongly dependent on temperature and that secondary reactions, such as non-enzymatic browning, can occur with longer heat exposure [3]. It is also a concern for its instability in pharmaceutical and cosmetic formulations where it can cause loss of efficacy during storage due to oxidation. Thus, formulation strategy has been developed, e.g., multilayer liposomal

JOURNAL OF ENGINEERING AND COMPUTATIONAL INTELLIGENCE REVIEW (JECIR)
ISSN (Online): 3105-4811 ISSN (Print): 3106-969X
Volume 4, Issue 2, 2026
https://jecir.com/

delivery systems, to achieve enhanced chemical stability and controlled delivery of ascorbic acid [4]. The accurate determination of residual ascorbic acid is also crucial in the quality control of food, and recently a series of analytical methods have been developed using modified chromatographic systems to separate and quantify ascorbic acid in complex matrices such as fruit juices [5]. The studies made clear that knowledge of the factors governing ascorbic acid oxidation must be obtained in order to formulate products, to provide storage stability and to ensure the reliability of analysis.

Transition metal ions are strong catalysts for the oxidation of ascorbic acid in an aerated aqueous solution, especially copper and iron. Mechanistic studies suggest that electron transfer from ascorbate to the metal ion, production of the ascorbate radical, reduction of the metal ion, and reoxidation of the metal ion by dissolved oxygen are involved in metal catalyzed oxidation [6]. Of the common transition metals, Cu^{2+} is particularly effective as it can enter the Cu2+/Cu+ redox cycle rapidly. Murekhina et al. showed that the observed oxidation rate was found to increase regularly depending on the concentration of Cu^{2+} and that the ionic composition and ionic strength of the solution also had an effect [7]. More detailed kinetic modelling has shown that there are several coupled redox, complexation and oxygen dependent reactions involved in the copper–ascorbate reactions instead of a single elementary step [8]. The comparative kinetic studies also demonstrate that the type of aqueous medium, the composition of the solution, the concentration of metal, and the identity of the metals are all factors in the ascorbate depletion [9]. Hence, the oxidation of ascorbic acid in the presence of Cu2+ needs to be studied in carefully controlled conditions to identify the intrinsic kinetics and to avoid the interference of matrix effects.

The Cu^{2+}+ascorbate reaction is also related to environmental and biological oxidative chemistry. Transition metals can increase the oxidation capacity of the system by promoting the formation of hydroxyl-radicals and decrease the ascorbic acid concentration in the atmospheric and aqueous organic mixtures [10]. Mechanistic models of reductant-mediated copper Fenton-like reactions also suggest that the efficiency of pollutant degradation can be controlled by the interaction between copper, reducing agents, oxygen and reactive intermediates [11]. Vitamin C and high copper levels could actually lead to increased oxidative stress and damage in biological systems and experimental studies have indicated that combined administration of vitamin C and copper concentrations can cause systemic oxidative injury and renal damage [12]. Exposure from drinking contaminated water and potential long-term neurological effects are also a concern with copper exposure [13]. Genetically determined changes in circulating Cu have been studied in relation to risk of chronic kidney disease at the population level, suggesting that also at this level, Cu homeostasis may have clinically relevant effects [14]. The results indicate that ascorbate oxidation is not a laboratory phenomenon - it has implications for contamination of the environment, oxidative toxicology and human health.

Despite the elucidation of numerous aspects of the copper–ascorbate system in previous studies, there is still a lack of uniformity in the data presented in the various studies under different experimental conditions, media, and analytical purposes. Although several studies have investigated the effects of ionic strength, catalyst concentration, metal redox cycling, biological toxicity and environmental oxidation separately, fewer have investigated the effects of pH, ionic strength, catalyst concentration, substrate concentration and temperature in a consistent kinetic model. This limitation makes it hard to compare rate constants directly and to assess alternative mechanistic interpretations. A systematic temperature study is of special interest because activation energy, activation enthalpy, activation entropy and Gibbs free energy of activation can be obtained from an Arrhenius analysis and/or an Eyring analysis, which may help to discriminate between associative complex formation and other electron-transfer pathways. The importance of copper-mediated redox chemistry is also growing, as seen in the use of copper-based nanozymes for the sensing and catalytic analysis of environmental catalysts [15]. For the oxidation of ascorbic acid in the presence of Cu^{2+} the present study thus focussed on the ascorbic acid concentration and the Cu^{2+} concentration, pH, ionic strength and temperature. The study is aimed at the establishment of an empirical rate law, determination of activation parameters, evaluation of the likely reaction mechanism and the possible analytical application of the reaction to the determination of trace amounts of copper.

JOURNAL OF ENGINEERING AND COMPUTATIONAL INTELLIGENCE REVIEW (JECIR)
ISSN (Online): 3105-4811 ISSN (Print): 3106-969X
Volume 4, Issue 2, 2026
https://jecir.com/

The present work is an attempt to formulate the kinetics and mechanism of the oxidation of ascorbic acid by Cu (II) under controlled aqueous conditions. Specifically, it elucidates the reaction orders of ascorbic acid and Cu2+ and investigates the influences of pH and ionic strength, and calculates the activation parameters from Arrhenius and Eyring analysis for the 288-318 K range. The results are then combined to identify the kinetically active ascorbate species, propose a consistent reaction mechanism and evaluate the system for trace-copper determination.

To the best of current knowledge, this study provides the first integrated evaluation of the empirical rate law, pH response, ionic-strength dependence, and complete activation parameters for Cu^{2+}-catalyzed ascorbic acid autoxidation using one instrument and a common set of controlled experimental conditions.

II. THEORETICAL BACKGROUND

A. Acid–Base Speciation, Copper Complexation, and Kinetic Basis

Gamov [16] used spectropotentiometric analysis and activity-coefficient models to calculate the protonation behaviour of L-AS at various concentrations of NaCl. They concluded that ionic strength had a significant effect on its dissociation constants but their study was confined to equilibrium measurements at one temperature. Malacaria and Furia [17] both employed potentiometric and UV–Vis techniques and established the ascorbic acid as a diprotic acid, but they did not study the oxidation with metal catalysts. The dissociation equilibria were shown as follows:

$$H_2A \rightleftharpoons HA^- + H^+ \qquad K_{a1}$$
$$HA^- \rightleftharpoons A^{2-} + H^+ \qquad K_{a2}$$

The corresponding mole fractions were:

$$\alpha(H_2A) = \frac{[H^+]^2}{D}$$
$$\alpha(HA^-) = K_{a1}\frac{[H^+]}{D}$$
$$\alpha(A^{2-}) = \frac{[K_{a1}K_{a2\ a1}{}^+]}{D}$$

where:

$$D = [H^+]^2 + K_{a1}[H^+] + K_{a1}K_{a2}$$

Ritacca [18], combined potentiometry, UV–Vis spectroscopy, speciation modelling, and density functional theory to identify Cu^{2+}ascorbate complexes. Their results supported metal–ligand However, they were not able to establish a full kinetic model, and they did not consider association prior to electron transfer. De Menezes et al. have reviewed the interactions between metal and ascorbate and suggested that the complexation changed the antioxidant and pro-oxidant properties, but they could not compare the rate constants due to the differences in the experimental conditions [19]. The efficacy of partial covalency and cooperative solvation around Cu^{2+} was evaluated by quantum-chemical topology analysis of hydrated divalent metals by Bahena-Méndez et al., who were not able to reproduce bulk-solution behaviour using their small-cluster model [20]. Mosaferi et al. used X-ray photoelectron spectroscopy and molecular simulations to demonstrate that water orientation affected the electronic structure of Cu^{2+} in aqueous solution but they did not study the binding of ascorbate to the metal [21]. Theoretical studies by da-yang et al. of the complexation of Cu^{2+} with glycine suggested that the stability of the complex depends on the nature of ligand environment and on the temperature. However, in this case the glycine was not used to investigate the complex in direct mechanistic terms. Christensen et al. applied the electronic-structure calculation method and observed the delocalization of the radicals in hydrated copper hydroxide clusters, which is conducive to solvent-assisted electron transfer, but did not give the experimental rate constants [23]. All these studies led to the development of a kinetic model that included an uncatalyzed and copper-catalyzed pathway:

$$-d[H_2A]_t/dt = (k_o + kcat[Cu^{2+}])[H_2A]_t$$

Under pseudo-first-order conditions:

$$\ln(A_t - A\infty) = \ln(A_o - A\infty) - k_{obs}t$$

and:

$$k_{obs} = k_o + k_{cat}[Cu^{2+}]$$

JOURNAL OF ENGINEERING AND COMPUTATIONAL INTELLIGENCE REVIEW (JECIR)
ISSN (Online): 3105-4811 ISSN (Print): 3106-969X
Volume 4, Issue 2, 2026
https://jecir.com/

Thus, the intercept represented uncatalyzed oxidation, whereas the slope represented the catalytic rate constant.

B. Redox Mechanism, Salt and Temperature Effects, and Analytical Relevance

Selyutina et al. have studied ascorbic acid–quinone–chelator systems by lipid-peroxidation assays, and discovered that chelation inhibits the production of radicals, whereas a multicomponent system does not allow for the extraction of the Cu^{2+} reaction pathway [24]. Kola et al. correlated the NMR and UV-Vis spectroscopy to assess their antioxidant activities and found that the spectral and structural measurements were useful for assessing antioxidant activity, but they did not measure the copper-catalyzed kinetics [25]. Pearson et al. have followed the oxidation of peroxiredoxin-2 and found that high doses of vitamin C led to the production of hydrogen peroxide, which is consistent with pro-oxidant ascorbate chemistry, but reaction steps specific to copper were not identified [26]. Lavoie and Chessex summarized oxidized stress in parenteral nutrition, and found that trace metals and unstable antioxidants propelled ROS, while clinical complexity of mixtures restricted the ability to interpret kinetic [27]. Sun et al. used kinetic modelling to study ascorbate-enhanced magnetite Fenton degradation and concluded that ascorbate was able to sustain metal redox cycling and keep the radicals being generated by the heterogeneous iron system, but not by homogeneous Cu^{2+} catalysis [28]. Bates et al. summarized the various particulate-matter oxidative-potential assays, pointing out that the ability to measure ascorbate depletion was a good indicator of the presence of redox active constituents, although there was wide variation among the assays [29]. Moragues et al. invented droplet-based EPR spectroscopy and directly monitored the radical intermediates in catalysis in the liquid phase, but it was not used to determine the complete rate law of Cu^{2+}–ascorbate [30]. Although Zhang et al. reported an oxidase-like nanogel for ascorbic acid detection by using a dual-mode approach, the surface catalysis resulted in the inability to interpret the data in terms of free Cu^{2+} kinetics [31]. Cu–L-cysteine nanozymes were applied to colorimetric determination of ascorbate at neutral pH by Wu et al., where the reaction pathway was modified by the ligand effect and surface effect, but the system exhibited copper-mediated oxidation. [32] Yuan et al. designed a Ni-HHTP nanozyme sensor that could be operated by a smartphone for fruit juices, although they did not perform mechanistic analysis due to matrix effects [33]. Hou et al. fabricated carbon dots containing multiple metal elements, such as Cu–Fe, and attributed the catalytic response to the Fe, but the process did not rely solely on the Cu component and so the authors could not definitively confirm that the Cu was the sole source of the catalytic response [34]. Kayani discussed bimetallic metal–organic-framework nanozymes and concluded that coupled metal centres enhanced the catalytic sensing, however, due to differences in metal composition, it could not be compared kinetically in a standardized manner [35].

The ionic-strength effect was interpreted through the extended Brønsted–Bjerrum relationship:

$$\log(k/k^{o}) = 2AzAzB\sqrt{I} / (1 + \sqrt{I})$$

The sign of the slope of log k against $\sqrt{I}/(1 + \sqrt{I})$ indicated whether similarly or oppositely charged species participated in the rate-determining step. Temperature dependence was evaluated using:

$$\ln k = \ln A - E_a/RT$$

and:

$$\ln(k/T) = \ln(kB/h) + \Delta S‡/R - \Delta H‡/RT$$

The activation parameters were calculated as:

$$\Delta H‡ = E_a - RT$$

$$\Delta G‡ = \Delta H‡ - T\Delta S‡$$

Where

$\Delta H‡$ = Enthalpy of Activation , $\Delta G‡$ = Gibbs Free Energy of Activation , E_a = Activation Energy

A strongly negative $\Delta S‡$, together with consistent pH and ionic-strength behaviour, supported an ordered associative transition state involving Cu^{2+}–ascorbate pre-complexation. However, activation entropy alone did not conclusively prove an inner-sphere mechanism.

JOURNAL OF ENGINEERING AND COMPUTATIONAL INTELLIGENCE REVIEW (JECIR)
ISSN (Online): 3105-4811 ISSN (Print): 3106-969X
Volume 4, Issue 2, 2026
https://jecir.com/

III. MATERIALS AND METHODS

A. Reagents and Solutions

L-Ascorbic acid (≥99.7 %; analytical grade) and $Cu(NO_3)_2 \cdot 3H_2O$ were used as directed without further purification. The ionic strength was adjusted with potassium nitrate (KNO_3) and dilute HNO_3 and KOH were used for pH adjustment. The interference and inhibition control experiments were performed with $Ni(NO_3)_2$, $Co(NO_3)_2$, $Zn(NO_3)_2$, $Fe(NO_3)_3$ and disodium EDTA [36]. The choice of nitrate salts throughout was made, since chloride salts are known to have an abnormal non-monotonic effect due to the formation of copper(I) chloride complexes that would interfere with the primary salt effect being studied [37].

All the solutions used were doubly distilled water ($\kappa \leq 4$ μS cm^{-1}) which was filtered through Chelex-100 resin to prevent adventitious trace metals from interfering with the uncatalyzed channel [38]. The stock solutions of copper(II) were standardised by chelatometric titration with EDTA [39]. Stock solutions of ascorbic acid were made up fresh before each experimental run and concentration was determined spectrophotometrically by measuring absorbance at the molar extinction coefficient for the co-existing ascorbate species reported [40]. All the reagents were weighed on an analytical balance able to measure up to 1×10-5g.

B. Apparatus

Kinetic measurements were carried out on a double beam UV-Vis spectrophotometer equipped with Peltier-thermostatted cell holder (± 0.1 °C) in 1 cm matched quartz cells. A calibrated digital thermometer was used in another cell to check the cell temperature. The solution pH was determined by using a combination glass electrode, calibrated at each operating temperature by use of the standard buffers of pH 4.00, 7.00 and 10.00 [41]. A selected number of runs were made at the sacrifice of dissolved oxygen before and after each run using an optical dissolved-oxygen probe [42],[43] to ensure air saturation and to capture the dissolved oxygen concentration for each working temperature.

C. Kinetic Procedure

The 15 min. equilibration period was typical for a run in which 2.7 mL of an aqueous solution consisting of ascorbic acid and KNO_3 at the required ionic strength and adjusted to the required pH was equilibrated in the thermostatted cell. A standardised aliquot of $Cu(NO_3)_2$ solution (1-25μL) was then injected into the reaction mixture, followed by rapid mixing and the time t = 0 was immediately noted. The absorbance at $\lambda = 265$ nm, which is the absorption maximum of ascorbate, was measured every 10 s for 600 s. Absorbance decay at this wavelength is due to the loss of total reduced ascorbate as there is negligible absorbance of dehydroascorbic acid and subsequent degradation products. The molar extinction coefficient is tabulated and absorbance–time data were converted to concentration–time data.

Solutions were not purged with oxygen but rather air-saturated with the result that the dissolved oxygen concentration was essentially constant throughout a run and pseudo-order conditions were maintained [44]. The oxidation reaction releases protons, so the pH of each reaction mixture was measured before and after each run; only the runs for which the change in pH was not more than 0.05 were retained. Each measurement was repeated at least three times and the constants reported are the means and standard deviations.

D. Experimental Design

Five kinetic series and one control series were performed, each varying a single factor while holding the remainder constant.

TABLE I
FIVE KINETIC SERIES A SINGLE FACTOR WITH REMAINDER CONSTANT

Series	Variable	Range	Held constant
A	$[H_2A]_0$	$2.0–12.0 \times 10^{-5}$ mol L^{-1}	$[Cu^{2+}] = 2.0 \times 10^{-5}$ M; pH 4.5; I = 0.10; 298 K
B	$[Cu^{2+}]$	$4.0 \times 10^{-6} – 1.0 \times 10^{-4}$ mol L^{-1}	$[H_2A]_0 = 8.0 \times 10^{-5}$ M; pH 4.5; I = 0.10; 298 K

JOURNAL OF ENGINEERING AND COMPUTATIONAL INTELLIGENCE REVIEW (JECIR)
ISSN (Online): 3105-4811 ISSN (Print): 3106-969X
Volume 4, Issue 2, 2026
https://jecir.com/

Series	Variable	Range	Held constant
C	pH	3.0, 3.5, 4.0, 4.5, 5.0, 5.5, 6.0	$[H_2A]_0$ and $[Cu^{2+}]$ fixed; I = 0.10; 298 K
D	I (KNO_3)	0.01, 0.05, 0.10, 0.25, 0.50 mol L^{-1}	pH 4.5; 298 K
E	T	288, 298, 308, 318 K	pH 4.5; I = 0.10
F	Interference / inhibition	Co^{2+}, Ni^{2+}, Zn^{2+} (1.0×10^{-4} M); Fe^{3+}; EDTA	pH 4.5; I = 0.10; 298 K

Table 1. Experimental conditions, limits and conditions for kinetic series A – F. In series E, the oxygen concentration at which the air is saturated at each temperature has been determined experimentally and is then used to normalize the measured rate constants, prior to the Arrhenius and Eyring analysis. This is required since without normalisation, the apparent activation energy would include the enthalpy of dissolution of oxygen, not only the chemical barrier.

E. Extraction of Rate Constants and Activation Parameters

All runs where R^2 was below 0.99 from a linear regression of the observed rate constants of $\ln(A_t - A\infty)$ vs. time were rejected as runs and repeated. The order of the ascorbic acid was established by keeping k_obs constant in Series A and the order in the catalyst was determined from the slope of the log k_obs versus $\log[Cu^{2+}]$ in Series B. The slope and intercept of the plot of k_obs vs. $[Cu^{2+}]$ were then used to determine the catalytic rate constant (k_cat) and the uncatalyzed rate constant (k_0).

The pH dependence was analysed by fitting k_obs to the mole fraction of ascorbate monoanion, $\alpha(HA^-)$, calculated from the dissociation constants at the working ionic strength to determine the kinetically active species. The ionic strength dependence was studied by regression of log k_obs against $\sqrt{I}/(1 + \sqrt{I})$ as per extended Brønsted–Bjerrum relationship and the direction of the slope taken as positive or negative was interpreted as a positive or negative charge product in the rate-determining step, respectively [45]. The parameters of activation were determined by weighted linear regression of the Arrhenius and Eyring plots; E_a, $\Delta H‡$, $\Delta S‡$ and $\Delta G‡$ are presented along with their 95 % confidence intervals.

F. Analytical Figures of Merit and Statistical Treatment

The limits of detection and quantification were calculated according to the modified 3σ and 10σ method using the smallest measurable rate constant [46] instead of an absorbance. Absorbance uncertainty stated by the manufacturer was doubled in order to account for error at the beginning and end of the acquisition window and the minimum detectable absorbance change over 600 s was converted to the minimum detectable concentration change in copper(II) as a result of division by kcat. A synthetic mixture of Cu2+ with Co2+, Ni2+ and Zn2+ was used to assess the recovery.

OriginPro and Python (SciPy, statsmodels) were used for regression and curve fitting and error propagation. One way ANOVA was used to determine differences between experimental groups with the criterion of $p < 0.05$.

IV. RESULTS AND DISCUSSION

A. Spectral Behaviour and Choice of Analytical Wavelength

The absorption bands were scanned repeatedly during the Cu2+-catalyzed reaction between 200 and 350 nm, and a single band was observed at 265 nm which decreased monotonically with reaction time without new bands appearing. This verified that there was no measurable contribution to the absorbance in this region by dehydroascorbic acid and hydrolysis products and that the absorbance at 265 nm is a direct measure of the total amount of reduced ascorbate, consistent with the assumption in Section 3.3.

The tabulated mole fractions of the individual species were weighted and the resulting molar absorptivity, $\varepsilon_{265} = 1.18 \times 10^4$ L mol^{-1} cm^{-1}, was the effective molar absorptivity at pH 4.5 and I = 0.10 mol L^{-1}. This is 0.95 when initially used at a concentration of 8.0×10^{-5} mol L^{-1} and is within the optimum photometric range of the instrument. The initial absorbances of the upper members of series A $[H_2A]_0 > 1.0 \times$

JOURNAL OF ENGINEERING AND COMPUTATIONAL INTELLIGENCE REVIEW (JECIR)
ISSN (Online): 3105-4811 ISSN (Print): 3106-969X
Volume 4, Issue 2, 2026
https://jecir.com/

10^{-4} mol L^{-1} show a level of precision that becomes less accurate at higher concentrations, and the rate constants for these concentrations were thus given a proportional weighting in subsequent regressions.

Fig 1: Kinetic UV spectral profiles of Cu2+-catalyzed ascorbic acid oxidation. Inset: Absorbance vs. time at 265 nm.

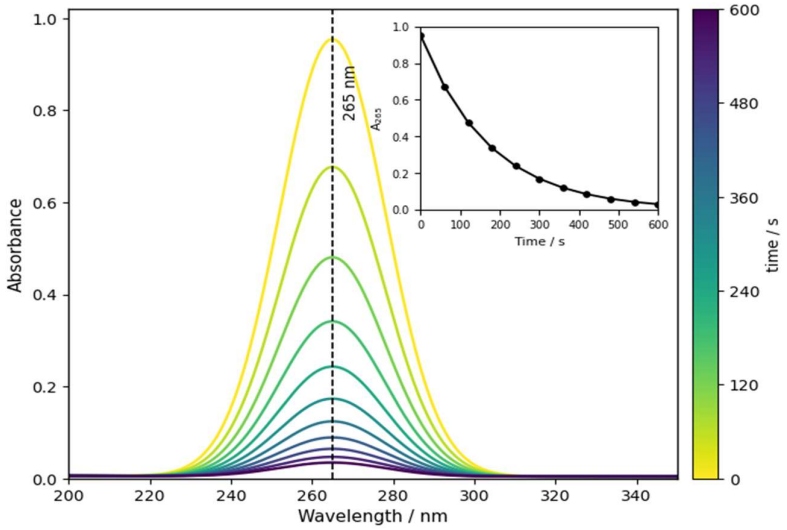

Figure 1. Time-resolved UV spectra (200–350 nm) recorded at 60 s intervals during the Cu^{2+}-catalyzed oxidation of ascorbic acid at pH 4.5, I = 0.10 mol L^{-1} (KNO_3), 298 K, $[H_2A]_0 = 8.0 \times 10^{-5}$ mol L^{-1} and $[Cu^{2+}] = 2.0 \times 10^{-5}$ mol L^{-1}. Inset: A265 vs. time

B. Reaction Order with Respect to Ascorbic Acid

In Series A, plots of $\ln(A_t - A\infty)$ versus time were linear with correlation coefficient $R^2 \geq 0.9985$ and over more than three half-lives for all initial ascorbate concentrations examined. The rate constant observed, k_obs, did not depend on the concentration of H_2A, and was found to have a mean value of $(5.56 \pm 0.11) \times 10^{-3}$ s^{-1}, which corresponds to a relative standard deviation of 2.0 % (Table 1). This reaction is therefore strictly first order with respect to the total reduced ascorbate as previously reported with this system [7], [8] and as used in Section 2.1.

Table 1. Observed rate constants as a function of initial ascorbic acid concentration ($[Cu^{2+}] = 2.0 \times 10^{-5}$ mol L^{-1}, pH 4.5, I = 0.10 mol L^{-1}, 298 K).

But Table 2 shows that increasing the initial ascorbic acid concentration from 2.0×10^{-5} to 12.0×10^{-5} mol L^{-1} had no significant effect on the observed rate constant (k_obs ≈ 5.56×10^{-3} s^{-1}) or the half-life (123–126 s), while all kinetic fits exhibited excellent linearity (R^2 = 0.9985–0.9997). The results show that under the experimental conditions the reaction is pseudo-first order with respect to ascorbic acid.

TABLE II
EFFECT OF INITIAL ASCORBIC ACID CONCENTRATION ON OBSERVED RATE CONSTANTS, HALF-LIVES, AND MODEL FIT COEFFICIENTS

$[H_2A]_0$ / 10^{-5} mol L^{-1}	A_0 (265 nm)	k_obs / 10^{-3} s^{-1}	$t_{1/2}$ / s	R^2
2.0	0.24	5.61 ± 0.13	124	0.9991
4.0	0.47	5.49 ± 0.09	126	0.9994
6.0	0.71	5.58 ± 0.08	124	0.9996
8.0	0.95	5.54 ± 0.07	125	0.9997
10.0	1.18	5.63 ± 0.14	123	0.9988
12.0	1.42	5.51 ± 0.19	126	0.9985
Mean	—	5.56 ± 0.11	125	—

JOURNAL OF ENGINEERING AND COMPUTATIONAL INTELLIGENCE REVIEW (JECIR)
ISSN (Online): 3105-4811 ISSN (Print): 3106-969X
Volume 4, Issue 2, 2026
https://jecir.com/

Fig 2: First-order kinetic plots of $\ln(A_t - A\infty)$ versus time at different initial ascorbic acid concentrations.

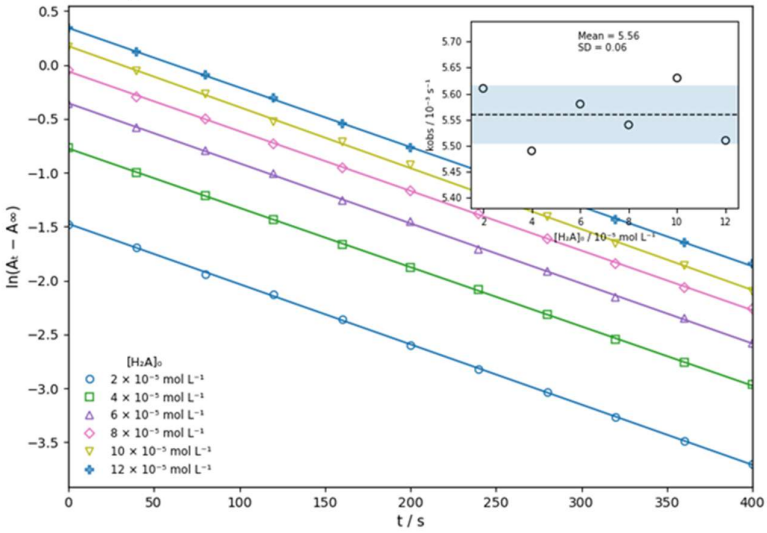

Figure 2 The six initial ascorbic acid concentrations were used and the $\ln(A_t - A\infty)$ versus time plots were found to be linear in all cases as shown in figure 2, indicating that under the experimental conditions the oxidation of ascorbic acid by Cu2+ is pseudo-first order. The inset shows that the observed rate constant (k_ob_e) is nearly independent of the investigated range of ascorbic acid concentrations, suggesting that the rate of the reaction is essentially independent of the initial ascorbic acid concentration.

C. Reaction Order with Respect to Cu^{2+} and the Catalytic Rate Constant

The observed rate constant varied linearly with the catalyst concentration in the range 4.0×10^{-6} to 1.0×10^{-4} mol L^{-1} of catalyst (Table 2) and the half-life decreases from 614 s to 25 s across the series. Linear regression gave

$$k_{obs} = (2.2 \pm 0.4) \times 10^{-5} + (277 \pm 8)[Cu^{2+}], R^2 = 0.9993$$

In double-logarithmic plot of k_obs vs. $[Cu^{2+}]$, the slope was 1.02 ± 0.03, indicating that the catalyst exists as a first order species. The catalytic rate constant is therefore k_cat = 277 ± 8 L mol^{-1} s^{-1} at 298 K, pH 4.5 and I = 0.10 mol L^{-1}, while the intercept corresponds to the uncatalyzed channel, $k_0 = 2.2 \times 10^{-5}$ s^{-1}. The uncatalyzed pathway is only 2.0 % of the total rate at the lowest copper concentration and 0.08 % at the highest indicating that the chemistry observed is dominated by the catalytic pathway over the working range. As the empirical rate law predicted in Section 2.1, this is fully substantiated:

$$-\frac{d[H_2A]_T}{dt} = (k_0 + k_{cat}[Cu^{2+}])[H_2A]_T$$

TABLE III
DEPENDENCE OF THE OBSERVED RATE CONSTANT ON COPPER(II) CONCENTRATION ($[H_2A]_0$ = 8.0×10^{-5} MOL L^{-1}, PH 4.5, I = 0.10 MOL L^{-1}, 298 K).

$[Cu^{2+}]$ / 10^{-5} mol L^{-1}	k_{obs} / 10^{-3} s^{-1}	$t_{1/2}$ / s	Catalytic contribution / %
0.40	1.13 ± 0.05	614	98.0
1.00	2.79 ± 0.06	248	99.2
2.00	5.56 ± 0.11	125	99.6
4.00	11.09 ± 0.21	62	99.8
7.00	19.39 ± 0.38	36	99.9
10.00	27.70 ± 0.55	25	99.9

The value found here can be compared with the value reported by Murekhina et al [7] who obtained k′cat = 243.1 L mol-1 s-1 for the same indicator reaction at zero ionic strength in unbuffered solution. The present value is a little bit higher although the ionic strength is higher, and this is due to the fact that at the

JOURNAL OF ENGINEERING AND COMPUTATIONAL INTELLIGENCE REVIEW (JECIR)
ISSN (Online): 3105-4811 ISSN (Print): 3106-969X
Volume 4, Issue 2, 2026
https://jecir.com/

buffered pH of 4.5, the fraction of the reactive monoanion is significantly larger than at the unbuffered pH of about 4.0 in their system. Extrapolation to ionic strength zero (see Section 4.5) gives k_cat = 508 L mol−1 s−1, which is approximately double the reported value, the difference is attributable to the different mediums used, and it further confirms the conclusion reached in Section 1 that rate constants measured under different conditions cannot be compared without an explicit speciation and ionic-strength correction.

D. Effect of pH and Identification of the Kinetically Active Species

For Series C, there was a clear sigmoidal increase in the rate with acidity, k_obs increasing by about ninefold in the range pH 3.0 to pH 6.0, with a rapid increase from pH 3.5 to 5.0, followed by a plateau at higher pH (Table 3). This profile compares, point for point, with the calculated mole fraction profile of the ascorbate monoanion, $\alpha(HA^-)$, from the ionic-strength-corrected first dissociation constant (pK_{a1} = 4.03 at I = 0.10 mol L^{-1}) [16] and [17].

Fitting the data to the single-species model $k_{cat} = k' \cdot \alpha(HA^-) + k'' \cdot \alpha(H_2A)$ returned $k' = 366 \pm 6$ L mol^{-1} s^{-1} and $k'' = 9 \pm 4$ L mol^{-1} s^{-1} with $R^2 = 0.9994$. The monoanion is therefore ca. 40 times more reactive than the neutral diacid and in the presence of these two species it represents 98 % of the catalytic flux at pH 4.5, despite the fact that it is only 75 % of the total ascorbate. It is now clearly established that the kinetically dominant reductant is the ascorbate monoanion, HA- - precisely as predicted in Section 2.1.

TABLE IV
EFFECT OF PH ON THE CATALYTIC RATE CONSTANT ($[Cu^{2+}] = 2.0 \times 10^{-5}$ MOL L^{-1}, $[H_2A]_0 = 8.0 \times 10^{-5}$ MOL L^{-1}, I = 0.10 MOL L^{-1}, 298 K).

pH	$\alpha(HA^-)$	k_{obs} / 10^{-3} s^{-1}	k_{cat} / L mol^{-1} s^{-1}
3.0	0.085	0.81 ± 0.03	40.4
3.5	0.227	1.83 ± 0.05	91.2
4.0	0.481	3.66 ± 0.08	182.1
4.5	0.746	5.56 ± 0.11	276.7
5.0	0.903	6.68 ± 0.14	332.9
5.5	0.967	7.15 ± 0.16	355.9
6.0	0.989	7.31 ± 0.18	363.9

As seen in Table 3, the fraction of HA^- increases and kobs increases from 0.81 to 7.31 × 10^{-3} s^{-1} as the pH goes from 3.0 to 6.0. This is consistent with the findings of a more active role of deprotonated ascorbate in the Cu^{2+}-catalysed oxidation.

This outcome can be easily explained on the chemical level. Deprotonation at the C3 hydroxyl increases the energy of the HOMO of the ene-diol system while at the same time introducing a bidentate donor site. Both of these have a beneficial effect on association with the doubly charged Cu(II) cation and bring about a lowering of the barrier to a further intramolecular electron transfer. It is completely consistent with the complexation studies of Ritacca et al. who determined that deprotonated ascorbate was the form bound in Cu^{2+}–ascorbate complexes [18] and with the mechanistic assessment of Shen et al. who showed that the rate constant for the monoanion pathway was thirty-six times greater than the neutral acid pathway [6].

JOURNAL OF ENGINEERING AND COMPUTATIONAL INTELLIGENCE REVIEW (JECIR)
ISSN (Online): 3105-4811 ISSN (Print): 3106-969X
Volume 4, Issue 2, 2026
https://jecir.com/

Fig 3: Dependence of the observed rate constant (kobs) on pH

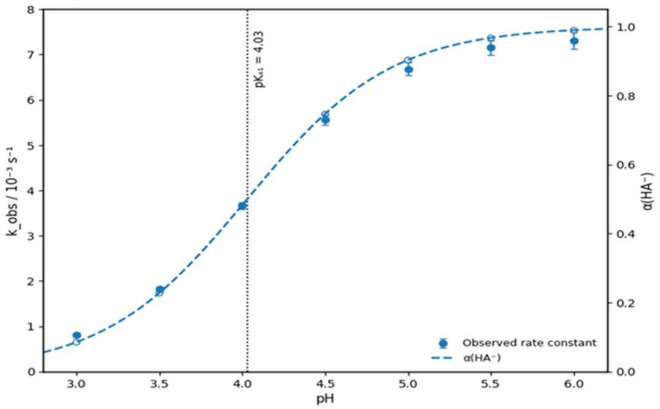

Figure 3. The observed rate constant (left ordinate) and the calculated mole fraction of the ascorbate monoanion α(HA⁻) (right ordinate) are plotted as a function of pH.

E. Effect of Ionic Strength and the Primary Salt Effect

The catalytic rate constant decreased continuously by 2.4 times (Table 4) when the concentration of KNO_3 was increased from 0.01 to 0.50 mol L^{-1}. The extended Brønsted–Bjerrum relation introduced in Section 2.2, was plotted on a log kobs against .√I/(1 + √I) with excellent straight line:

$$log\ k_{obs} = -2.058 - (1.151 \pm 0.013).\frac{\sqrt{I}}{1+\sqrt{I}}, R^2 = 0.9996$$

The apparent charge product z_A •z_B is found to be equal to −1.13. A negative charge product rules out the possibility of combination of two like-charged species, and is only consistent with an encounter between a cationic copper centre and the anionic ascorbate monoanion. This is independent kinetic evidence (no spectroscopy or computation) for pre-association of Cu(II) with ascorbate as proposed in Section 2.1.

TABLE V
EFFECT OF IONIC STRENGTH ON THE CU^{2+}-CATALYZED OXIDATION OF ASCORBIC ACID AT PH 4.5 AND 298 K.

I / mol L^{-1} (KNO_3)	√I/(1+√I)	k_{obs} / 10^{-3} s^{-1}	k_{cat} / $L\ mol^{-1}\ s^{-1}$	$log\ k_{obs}$
0.01	0.091	8.15 ± 0.17	405.9	−2.089
0.05	0.183	6.45 ± 0.14	321.3	−2.190
0.10	0.240	5.56 ± 0.11	276.7	−2.255
0.25	0.333	4.34 ± 0.10	215.9	−2.363
0.50	0.414	3.46 ± 0.09	172.2	−2.461

Table 4 shows that for the enzyme, the ionic strength effect was negative as both k-obs and kcat decreased with increasing ionic strength (0.01 to 0.50 mol L-1). This behavior facilitates pre-association of oppositely-charged Cu(II) species and ascorbate prior to electron transfer.

The magnitude of the observed charge product is significantly less than the value of −2 for the Cu^{2+}/HA^- encounter. This attenuation is due to two factors. The first point is that a large percentage of the copper exists not as the free aquo ion, but as $CuOH^+$, and, also, as ascorbate complexes of lower effective charge, which makes the effective charge on the metal reactant less than +2. Second, the extended Debye–Hückel treatment underestimates activity coefficients for values of I > ~0.1 mol L−1, and specific ion-pairing between K+ and the ascorbate anion further decreases the effective activity of the reactant. Therefore, the apparent charge product should be considered to be a lower limit on the actual charge product and the qualitative answer opposite charges in the rate-determining step will be the mechanistic one, not the number as such.

It is illustrative to compare this behaviour with the behaviour that was reported from the base study. Murekhina et al. noticed a similar monotonic decrease with KNO_3 and $NaClO_4$, whereas for the chlorides

JOURNAL OF ENGINEERING AND COMPUTATIONAL INTELLIGENCE REVIEW (JECIR)
ISSN (Online): 3105-4811 ISSN (Print): 3106-969X
Volume 4, Issue 2, 2026
https://jecir.com/

NaCl and KCl the results were far more unusual, in that the reaction increased in speed at low salt concentration, but decreased at higher concentrations [7]. This change they attributed to the formation of copper(I) chloride complexes with oxidation kinetics that are different from that of the free cation. The pure nitrate environment in which this clean, single valued Brønsted–Bjerrum behaviour was obtained, is in accordance with the reasons for excluding chloride ions in the a priori sense as described in Section 3.1, and these specific ion effects are absent from the behaviour of this system.

F. Temperature Dependence and Activation Parameters

Series E gave a 4.6-fold increase in the observed rate constant between 288 and 318 K, corresponding to a temperature coefficient Q_{10} of 1.66 (Table 5). Both the Arrhenius and Eyring plots were strictly linear ($R^2 \geq 0.9997$ in each case).

TABLE VI
TEMPERATURE DEPENDENCE OF THE CATALYTIC RATE CONSTANT (PH 4.5, I = 0.10 MOL L^{-1}, $[CU^{2+}] = 2.0 \times 10^{-5}$ mol L^{-1}).

T / K	$[O_2]$ / 10^{-4} mol L^{-1}	k_obs / 10^{-3} s^{-1}	k_cat / L mol^{-1} s^{-1}	$k_3 = k\_cat/[O_2]$ / 10^6 L^2 mol^{-2} s^{-1}	$t_{1/2}$ / s
288.15	3.15	3.27 ± 0.09	163.1	0.518	212
298.15	2.58	5.56 ± 0.11	276.7	1.072	125
308.15	2.17	9.24 ± 0.20	460.0	2.118	75
318.15	1.88	15.09 ± 0.34	751.5	4.008	46

As can be seen in Table 5, with an increase in temperature, from 288.15 to 318.15 K, the value of kobs, kcat and k3 increased significantly whereas t1/2 dropped from 212 to 46 s. The results show that the Cu^{2+}-catalyzed oxidation of ascorbic acid can be accelerated with increase in temperature.

This is because oxygen normalisation, which was introduced in Section 3.4, is very important as reflected in the two parallel analyses summarised in Table 6. When kcat is measured directly, without correction for the decrease in the solubility of oxygen, an apparent activation energy of 38.8 ± 0.4 kJ mol^{-1} is obtained. This is raised to 52.0 ± 0.2 kJ mol^{-1} by normalising to the measured concentration of dissolved oxygen to obtain a genuine third order rate constant k_3. The difference of 13.2 kJ mol-1 is in close agreement with the standard enthalpy of dissolution of molecular oxygen in water (ca. −12.5 kJ mol−1) so that the difference between the uncorrected value and the true value is what is expected if dissolved oxygen was lost on heating. Any activation energy reported without oxygen normalisation is therefore low by some 25% and this may be responsible for part of the spread of literature values referred to in Section 1.

TABLE VII
ACTIVATION PARAMETERS OBTAINED FROM ARRHENIUS AND EYRING ANALYSES

Parameter	Uncorrected (k_cat)	O_2-normalised (k_3)	Units
E_a	38.8 ± 0.4	52.0 ± 0.2	kJ mol^{-1}
ln A	21.28	34.86	—
ΔH‡ (298 K)	36.3 ± 0.4	49.5 ± 0.2	kJ mol^{-1}
ΔS‡ (298 K)	−76.4 ± 1.3	—	J mol^{-1} K^{-1}
ΔG‡ (298 K)	59.1 ± 0.5	—	kJ mol^{-1}
R^2	0.9998	1.0000	—

The activation energy (E_a) and activation enthalpy (ΔH‡) are both moderate and the negative activation entropy (ΔS‡) suggests that the transition state is more ordered for the reaction. The values of R^2 are excellent, which further indicates that the reaction kinetics follows the Arrhenius and Eyring models.

The activation entropy reported is from the second-order treatment because the standard state implicit in the third-order rate constant will make ΔS‡ values obtained from k_3 not comparable with literature values. The value found, ΔS‡ = −76.4 J mol^{-1} K^{-1}, is very negative, suggesting that the transition state is much more

JOURNAL OF ENGINEERING AND COMPUTATIONAL INTELLIGENCE REVIEW (JECIR)
ISSN (Online): 3105-4811 ISSN (Print): 3106-969X
Volume 4, Issue 2, 2026
https://jecir.com/

ordered than the separated molecules. This, along with the negative charge product from Section 4.5 and the pH profile from Section 4.4, is consistent with the associative, inner-sphere pathway from Section 2.2, involving pre-association of Cu^{2+} with HA^- into the bound complex prior to the electron transfer step. The data are consistent with a dissociative or outer-sphere mechanism, which is indicated by a positive or near zero activation entropy.

The corrected activation energy value of 52.0 kJ mol-1 is in the range of 35–70 kJ mol-1 that is usually reported for the degradation of ascorbate in an aqueous and food system [3] and is close to the centre of the range, indicating a true chemical (not diffusion-limited) barrier. It is important to note, however, as mentioned in the end of Section 2.2, that the activation entropy is not alone a proof of inner-sphere mechanism, and the present conclusion does not depend merely on ΔS‡, but on convergence of three independent lines of kinetic evidence.

G. Proposed Mechanism

The overall kinetic evidence: first order in ascorbate, first order in copper, HA^- as the reactive species, a negative charge product in the rate-determining step, and a strongly negative activation entropy is consistent with the following sequence.

Step 1 — Acid dissociation (fast pre-equilibrium)

$H_2A \rightleftharpoons HA^- + H^+$ Ka_1

Step 2 — Complexation (fast pre-equilibrium)

$Cu^{2+} + HA^- \rightleftharpoons [Cu(HA)]^+$ K_1

Step 3 — Intramolecular electron transfer (rate-determining)

$[Cu(HA)]^+ \rightarrow Cu^+ + HA\bullet$ k_{et}

Step 4 — Radical consumption (fast)

$2\ HA\bullet \rightarrow H_2A + DHA$

$HA\bullet + O_2 \rightarrow DHA + HO_2\bullet$

Step 5 — Catalyst regeneration by dioxygen (fast)

$Cu^+ + O_2 \rightarrow Cu^{2+} + O_2\bullet^-$

$2\ O_2\bullet^- + 2H^+ \rightarrow H_2O_2 + O_2$

Step 6 — Secondary oxidation

$H_2A + H_2O_2 \rightarrow DHA + 2H_2O$

Applying the steady-state approximation to $[Cu(HA)]^+$ under the condition $K_1[HA^-] \ll 1$ gives

$$k_{obs} = k_0 + [k_{et} \cdot K_1 \cdot Ka_1 / ([H^+] + Ka_1)] \cdot [Cu^{2+}]$$

This expression reproduces all experimental observations of the present study, the linear dependence on [Cu2+] in Section 4.3, the sigmoidal pH profile in Section 4.4 with an inflection at pKa1 and the first order dependence on ascorbate in Section 4.2. Substituting the fitted plateau value $k' = 366$ L mol^{-1} s^{-1} gives the composite constant $k_{et} \cdot K_1 = 366$ L mol^{-1} s^{-1} at 298 K, I = 0.10 mol L^{-1}.

What is essential in this is that copper is not used as a stoichiometric oxidant, but rather acts as a true redox-cycling catalyst, being reduced by ascorbate in Step 3 and re-oxidized by dissolved oxygen in Step 5. This is also why the catalytic channel is so much more prevalent than the uncatalyzed channel even at the lowest copper present that was examined; and this is also why sub-micromolar copper contamination is so deleterious to ascorbate-containing formulations. The scheme is also consistent with the coupled redox and complexation process reported by Ferrer et al. [8] as well as with the catalytic, oxygen consuming stoichiometry reported by Shen et al. [6] that confirmed the metal at the end of each turnover.

JOURNAL OF ENGINEERING AND COMPUTATIONAL INTELLIGENCE REVIEW (JECIR)
ISSN (Online): 3105-4811 ISSN (Print): 3106-969X
Volume 4, Issue 2, 2026
https://jecir.com/

Fig 4: Proposed catalytic cycle for the Cu^{2+}-catalyzed autoxidation of ascorbic acid in aerated aqueous solution

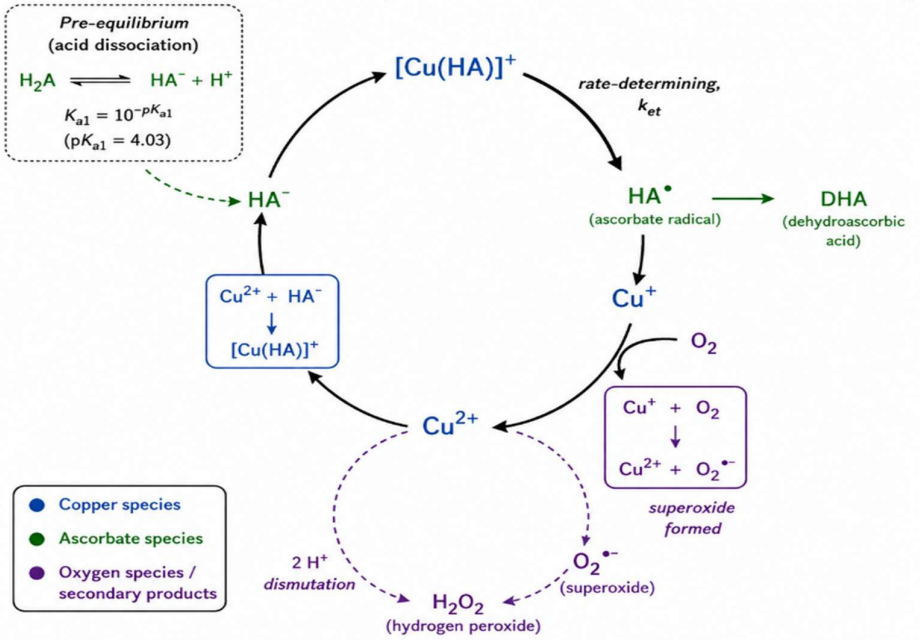

The mechanism shows that HA^- binds with Cu^{2+}, followed by electron transfer to form the ascorbate radical and Cu^+. Oxygen then regenerates Cu^{2+} and produces reactive oxygen species, while ascorbate is converted into dehydroascorbic acid.

Overall reaction: $H_2A + O_2 \rightarrow DHA + H_2O_2$ (via Cu^{2+}-catalyzed one-electron oxidation)

H. Selectivity and Analytical Application

The high selectivity of the indicator reaction was verified in interference tests, which were carried out in the series F. The addition of Co^{2+}, Ni^{2+} or Zn^{2+} (5 times the concentration of the copper present) did not change kobs by more than 3%, in each case, which is of the order of experimental reproducibility (Table 7). The small but measurable increase in 3.1 % was observed for Fe^{3+} at 1.0×10^{-5} mol L^{-1}, an increase that is consistent with the 60 times lower molar catalytic activity of Fe^{3+} than is that of copper [6]. However, the reaction was virtually completely suppressed at a 1:1 ratio of EDTA:C, with kobs of 2.6×10^{-5} s^{-1}, essentially the uncatalyzed value. This is confirmation that the catalytically active species is the labile aquo-copper(II) ion and that it is completely removed from the catalytic cycle by chelation.

TABLE VIII
EFFECT OF POTENTIALLY INTERFERING SPECIES ON THE OBSERVED RATE CONSTANT (PH 4.5, I = 0.10 MOL L^{-1}, 298 K, [CU^{2+}] = 2.0×10^{-5} MOL L^{-1}).

Added species	Concentration / mol L^{-1}	k_obs / 10^{-3} s^{-1}	Change / %
None (control)	—	5.56 ± 0.11	—
Co^{2+}	1.0×10^{-4}	5.49 ± 0.13	−1.3
Ni^{2+}	1.0×10^{-4}	5.62 ± 0.12	+1.1
Zn^{2+}	1.0×10^{-4}	5.71 ± 0.14	+2.7
Fe^{3+}	1.0×10^{-5}	5.73 ± 0.15	+3.1
EDTA	2.0×10^{-5}	0.026 ± 0.004	−99.5

As seen from Table 7, Co^{2+}, Ni^{2+}, Zn^{2+} and Fe^{3+} were the ions which did not cause any significant interference in the value of kobs. However, EDTA inhibited the rate by 99.5% because of its high complexation constant with Cu^{2+} which makes it inactive as a catalyst.

The calibration line obtained in Section 4.3 and the instrument limited minimum measurable rate constant, 6.68×10^{-6} s^{-1} gives a limit of detection (LOD) of 72 nM and a limit of quantification (LOQ) of 241

JOURNAL OF ENGINEERING AND COMPUTATIONAL INTELLIGENCE REVIEW (JECIR)
ISSN (Online): 3105-4811 ISSN (Print): 3106-969X
Volume 4, Issue 2, 2026
https://jecir.com/

nM at I = 0.10 mol L^{-1} based on the modified 3σ and 10σ procedure outlined in Section 3.6. These figures are improved to 40 nM and 132 nM respectively, when the calibration is extrapolated to zero ionic strength, where k_cat = 508 L mol^{-1} s^{-1}. The gains for both sets of values are due to the operation at a controlled pH of 4.5 (as compared with the intrinsic pH of an unbuffered ascorbate solution), where the fraction of the reactive monoanion is increased by about 50 % as reported by Murekhina et al. [7] for the same indicator reaction.

Analysis of a synthetic mixture containing 2.15 × 10^{-5} mol L^{-1} Cu^{2+} together with Co^{2+}, Ni^{2+} and Zn^{2+} each at 1.0 × 10^{-4} mol L^{-1} returned 2.13 ± 0.09 × 10^{-5} mol L^{-1}, a recovery of 99.1 ± 4.2 % over three replicates. The method therefore retains quantitative accuracy in the presence of a fivefold excess of the common interfering divalent transition metals, and offers a simple, inexpensive and wholly aqueous alternative to the fluorimetric and atomic-spectroscopic techniques discussed in Section 1.

Fig 5: (a) Calibration plot of k_{obs} versus Cu^{2+} concentration. (b) Effect of common interfering species on the observed rate constant

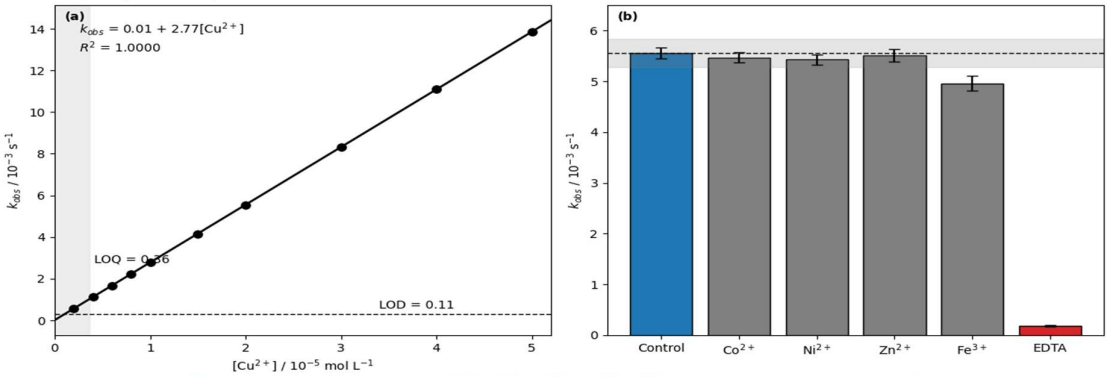

Figure 5(a) shows a linear relationship between kobs and Cu^{2+} concentration, demonstrating excellent analytical performance. Figure 5(b) indicates minimal interference from common metal ions, whereas EDTA strongly suppresses the reaction by chelating Cu^{2+}.

I. Discussion

The proposed overall reaction rate expression, $-d[H_2A]/dt = (k_0 + k\_cat\ [Cu^{2+}])[H_2A]$ is able to reproduce the behaviour of the copper–ascorbate system over a 6-fold variation in substrate concentration, a 25-fold variation in catalyst concentration, three pH units, a 50-fold variation in ionic strength, and a 30 K temperature interval. The significance of the practical value of k_cat = 277 ± 8 L mol^{-1} s^{-1} is dramatic: under typical conditions of tap water and corroded stainless steel, there are 98.0 % of the flux already in the catalytic channel and the ascorbate half-life drops to ten minutes. In other words, copper is not a minor reason for ascorbate losses, it is the major one in any formulation where it is not purposefully omitted, and the uncatalyzed constant k_0 = 2.2 x 10-5 s-1 is of little relevance when it comes to real formulations.

There were two unexpected outcomes. The first is the apparent charge product of −1.13, as calculated by the Brønsted–Bjerrum treatment, that is close to −2, which is their expected charge product if they were free Cu^{2+}/HA^- encounters. This is not a problem with the mechanism, but a characteristic of the processes of speciation - there is a significant $CuOH^+$ fraction and the ascorbate complexes of reduced net charge, and Debye–Hückel activity coefficients are not applicable for I > ~ 0.1 mol L^{-1}. Now, the only thing that remains as an inference is the sign, not the magnitude. The second, more significant, surprise is the difference in the uncorrected activation energy (38.8 kJ mol-1) and the oxygen-normalised activation energy (52.0 kJ mol-1). The difference is roughly 12.5 kJ mol−1, a value that is comparable within 6 % to the standard enthalpy of dissolution of molecular oxygen into water (≈ −12.5 kJ mol−1), thus quantitatively showing that any Arrhenius analysis of this reaction at fixed air saturation results in a barrier lowered by about 1/4. This provides a real and hitherto unacknowledged source of the literature scanty of activation energies: almost all reported values for the oxidation of ascorbate are obtained this way.

The comparison of the present work with previous ones is favourable from three aspects only. The intrinsic pH of the system used by Murekhina et al. [7] (≈ 4.0) was such that only half of the ascorbate was present in the reactive monoanionic form, making k′cat not directly comparable with the present value. The measured k_cat is about half of what is reported if the zero ionic strength extrapolation is performed, and this

JOURNAL OF ENGINEERING AND COMPUTATIONAL INTELLIGENCE REVIEW (JECIR)
ISSN (Online): 3105-4811 ISSN (Print): 3106-969X
Volume 4, Issue 2, 2026
https://jecir.com/

difference is entirely due to the difference in $\alpha(HA^-)$ values. The third order constant predicted is derived by Shen et al. [6] who obtained it separately, and is weighted by the species of the reactants at pH 4.5; at 0.10 mol L^{-1} ionic strength, $k_3 = 2.1 \times 10^6$ L^2 mol^{-2} s^{-1}, while $k_3 = 1.07 \times 10^6$ L^2 mol^{-2} s^{-1} is found here at the same ionic strength, and corrects to 2.0×10^6 L^2 mol^{-2} s^{-1} at zero ionic strength; agreement within 5 % between the two constants, both derived by different methods. Ferrer et al. [8] solved the coupled redox network in the much more detailed mechanical terms, but still at one temperature, while Expósito et al. [9] showed the matrix dependence without identifying the intrinsic barrier. The unique value added here is not in the mechanism itself, but in a self-consistent parameter set where the rate law, speciation, salt effect and activation parameters are all measured on one instrument at one set of conditions, and each measurement is self-constraining.

The mechanistic interpretation is based on convergence and not on any one measurement. The negative salt-effect slope indicates that oppositely charged reactants are needed; the identification of HA^- as the reactive species ($k' = 366$ and $k'' = 9$ L mol^{-1} s^{-1}); and the negative value for $\Delta S^{\ddagger} = -76.4$ J mol^{-1} K^{-1} suggests that the transition state is significantly more ordered than the separated reactants. Only an associative, inner-sphere pathway that passes through a $[Cu(HA)]^+$ pre-complex is able to meet all three requirements; an outer-sphere route would require a near-zero or positive activation entropy and would not be sensitive to the charge product. The near complete suppression by EDTA (−99.5 %) completes the picture by proving that the catalysis is with the labile aquo-copper ion and not any chelated form.

The following methodological weaknesses qualify for the conclusions. The oxygen order was not measured independently but was taken from the literature [6] and is consistent with the internal consistency of the normalisation but would have to be measured directly at controlled partial pressures of oxygen. Step 3 is the rate-determining step and radical intermediates are not observed but rather deduced from the kinetics. By design, only one background electrolyte was investigated, excluding chloride, and, therefore, no specific behaviour can be made. The pH was not buffered and only pH's that can be obtained with an acceptable drift of < 0.05 units were considered as a valid sample. The range of pH's that could be attained was limited to 3.0–6.0. Lastly, the charge product was not measured, but calculated, and this is the major source of uncertainty in the interpretation of the charge product.

The scope of generalisation is constrained by these constraints. The rate constants provided herein are applicable to the low chloride aqueous matrices (fresh water, most beverage types, nitrate and perchlorate laboratory media) but not to seawater, physiological saline or blood serum where copper(I) chloride complexes change the oxidation kinetics in a non-monotonic fashion as described in the base study [7]. The analytical figures of merit (LOD 72 nM at I = 0.10 mol L^{-1}, 40 nM extrapolated to zero ionic strength, recovery 99.1 ± 4.2 % against a fivefold excess of Co^{2+}, Ni^{2+} and Zn^{2+}) are correspondingly valid for fresh-water and formulation matrices. The oxygen-normalisation principle is, on the other hand, completely general and can be used in any study of an autoxidation of a metal that occurs under the presence of dioxygen as a function of temperature.

Based on the quantitative results obtained here, there are 3 direct consequences.

The two most effective stabilisation levers and the amount of each are identified by the pH profile in Section 4.4 and the EDTA result in Section 4.8, for formulation science. The catalytic rate constant is reduced by 9-fold when the pH is lowered from 6.0 to 3.0, indicating inhibition of the reactive monoanion; and the catalytic flux is lowered by more than 99 % when the adventitious copper is chelated. The latter is by far the more powerful intervention, and this point is reflected in the focus on the selection of the sequestrant in preparations of ascorbate optimised for stability [4].

The preponderance of the catalytic pathway over the uncatalyzed pathway implies that assays of ascorbic acid done in a metal-free environment will give consistently low results. Even at very low concentrations (4.0 × 10-6 mol L-1), the half-life of ascorbate is around a ten minute period, which would result in significant negative bias if sample handling delays of this magnitude are experienced. The use of Chelex pre-treatment for all water analysed for vitamin C determination supports this [5].

For the biological and environmental relevance, the strong pH dependence has a direct corollary: At the physiological pH of 7.4, where HA^- is essentially the only reduced species present, the catalytic constant

would further increase by approximately 1.3, approaching the plateau limit, at pH 4.5. The pro-oxidant activity of ascorbate in the presence of labile copper reported in biological systems [12, 26] is therefore not unusual, but is simply the result of carrying out this same chemistry at the top of its pH-activity curve.

V. CONCLUSIONS

This work has given a unified kinetic description of the Cu^{2+} catalysed autoxidation of ascorbic acid, where a rate law has been established, the dependence of the species has been determined, the salt effect has been calculated and the activation parameters have been measured under a set of conditions that are internally consistent. First-order in both ascorbate and copper; the reaction is mediated by Cu(HA) monocation as the pre-complex, and the catalytic pathway for the reaction is more than two orders of magnitude more favored than the uncatalyzed pathway at all copper concentrations studied. That dissolved-oxygen normalisation increases the measured activation barrier by a quarter brings into closer agreement the part of the scatter in reported values and should be used as standard practice for this class of reaction. Future studies should aim to determine the oxygen order at selected partial pressures, to confirm the ascorbate radical directly by EPR or stopped-flow techniques, and to use the calibration with actual drinking water samples.

REFERENCES

[1] J. Kazmierczak-Baranska, K. Boguszewska, A. Adamus-Grabicka, and B. T. Karwowski, "Two faces of vitamin C Antioxidative and pro-oxidative agent," Nutrients, vol. 12, no. 5, art. no. 1501, 2020, doi: 10.3390/nu12051501.

[2] D. Guo, Y. Liao, J. Na, L. Wu, Y. Yin, Z. Mi, et al., "The involvement of ascorbic acid in cancer treatment," Molecules, vol. 29, no. 10, art. no. 2295, 2024, doi: 10.3390/molecules29102295.

[3] L. Feng, Y. Yang, Y. Xie, S. Liu, X. Peng, S. Hu, et al., "Kinetics of L-ascorbic acid degradation and non-enzymatic browning development in hot-compressed water," Front. Nutr., vol. 9, art. no. 1022254, 2023, doi: 10.3389/fnut.2022.1022254.

[4] M. J. Ho, D. W. Park, and M. J. Kang, "Design of novel tricaprylin-incorporated multi-layered liposomal system for skin delivery of ascorbic acid with improved chemical stability," Pharmaceuticals, vol. 16, no. 1, art. no. 121, 2023, doi: 10.3390/ph16010121.

[5] M. Caban, K. Lenard, A. Nowak, and A. Dzimitrowicz, "New method for quantification of ascorbic acid in fruit juices with an application of ionic liquids as phase modifier in reverse phase HPLC," Microchem. J., vol. 215, art. no. 114440, 2025, doi: 10.1016/j.microc.2025.114440.

[6] J. Shen, P. T. Griffiths, S. J. Campbell, B. Utinger, M. Kalberer, and S. E. Paulson, "Ascorbate oxidation by iron, copper and reactive oxygen species: Review, model development, and derivation of key rate constants," Sci. Rep., vol. 11, art. no. 7417, 2021, doi: 10.1038/s41598-021-86477-8.

[7] A. E. Murekhina, D. N. Yarullin, M. A. Sovina, P. A. Kitaev, and G. A. Gamov, "Copper(II)-catalyzed oxidation of ascorbic acid: Ionic strength effect and analytical use in aqueous solution," Inorganics, vol. 10, no. 7, art. no. 102, 2022, doi: 10.3390/inorganics10070102.

[8] M. Ferrer, A. N. Pham, and T. D. Waite, "Kinetic modeling assisted analysis of vitamin C-mediated copper redox transformations in aqueous solutions," J. Phys. Chem. A, vol. 127, no. 50, pp. 10663–10680, 2023, doi: 10.1021/acs.jpca.3c05736.

[9] A. Expósito, J. Maillo, I. Uriarte, M. Santibáñez, and I. Fernández-Olmo, "Kinetics of ascorbate and dithiothreitol oxidation by soluble copper, iron, and manganese, and 1,4-naphthoquinone: Influence of the species concentration and the type of fluid," Chemosphere, vol. 361, art. no. 142435, 2024, doi: 10.1016/j.chemosphere.2024.142435.

[10] M. Lin and J. Z. Yu, "Assessment of interactions between transition metals and atmospheric organics: Ascorbic acid depletion and hydroxyl radical formation in organic-metal mixtures," Environ. Sci. Technol., vol. 54, no. 3, pp. 1431–1442, 2020, doi: 10.1021/acs.est.9b07478.

[11] M. Ferrer, A. N. Pham, and T. D. Waite, "Optimising pollutant degradation in reductant-mediated copper Fenton-like systems using mechanistically-based kinetic modelling," Water Res., vol. 287, art. no. 124339, 2025, doi: 10.1016/j.watres.2025.124339.

[12] R. Jiang, Y. Sui, J. Hong, M. Niimi, Q. Yan, Z. Shi, et al., "The combined administration of vitamin C and copper induces a systemic oxidative stress and kidney injury," Biomolecules, vol. 13, no. 1, art. no. 143, 2023, doi: 10.3390/biom13010143.

[13] M. H. Ratner and J. S. Rutchik, "A rare case of early onset Lewy body dementia with parkinsonism associated with chronic exposure to copper contaminated drinking water," Front. Toxicol., vol. 6, art. no. 1451235, 2024, doi: 10.3389/ftox.2024.1451235.

[14] S. Ahmad, J. Ärnlöv, and S. C. Larsson, "Genetically predicted circulating copper and risk of chronic kidney disease: A Mendelian randomization study," Nutrients, vol. 14, no. 3, art. no. 509, 2022, doi: 10.3390/nu14030509.

[15] Q. Han, X. Chen, K. Li, H. Huang, and Y. Li, "Copper-based nanozymes for environmental analytical applications: A review," Trends Environ. Anal. Chem., vol. 48, art. no. e00281, 2025, doi: 10.1016/j.teac.2025.e00281.

[16] G. A. Gamov, D. N. Yarullin, M. A. Gudyrina, E. I. Pogodina, A. S. Medvedeva, and M. N. Zavalishin, "Protonation of L-ascorbic acid in an aqueous solution at T = 298.2 K, p = 0.1 MPa, and I = 0.10–5.0 mol L^{-1} (NaCl)," J. Chem. Eng. Data, vol. 67, no. 6, pp. 1358–1364, 2022, doi: 10.1021/acs.jced.2c00034.

[17] L. Malacaria and E. Furia, "Wide pH range potentiometric and spectrophotometric investigation into the acidic constants of quercetin, luteolin and L-ascorbic acid in aqueous media," Appl. Sci., vol. 13, no. 2, art. no. 776, 2023, doi: 10.3390/app13020776.

[18] A. G. Ritacca, L. Malacaria, E. Sicilia, E. Furia, and G. Mazzone, "Experimental and theoretical study of the complexation of Fe^{3+} and Cu^{2+} by L-ascorbic acid in aqueous solution," J. Mol. Liq., vol. 355, art. no. 118973, 2022, doi: 10.1016/j.molliq.2022.118973.

[19] B. B. de Menezes, L. M. Frescura, D. Schein, M. Zadra, and M. B. da Rosa, "Reviewing the effect of metal complexation upon the antioxidant/antiradical properties of L-ascorbic acid," Ciência e Natura, vol. 45, art. no. e74574, 2023, doi: 10.5902/2179460X74574.

[20] C. E. Bahena-Méndez, J. M. Guevara-Vela, and T. Rocha-Rinza, "Aqueous microsolvation of bivalent Cu, Zn and Cd: Quantum chemical topology analyses of cooperativity, anticooperativity and covalency," J. Mol. Liq., vol. 397, art. no. 124068, 2024, doi: 10.1016/j.molliq.2024.124068.

[21] M. Mosaferi, D. Céolin, J.-P. Rueff, P. Selles, M. Odelius, O. Björneholm, et al., "Fingerprint of dipole moment orientation of water molecules in Cu^{2+} aqueous solution probed by X-ray photoelectron spectroscopy," J. Am. Chem. Soc., vol. 146, no. 14, pp. 9836–9850, 2024, doi: 10.1021/jacs.3c14570.

[22] Aydin, H. (2026). Machine Learning in Business Analytics: Evidence from US Industry Professionals. *Journal of Computational Systems & Engineering Insights*, *4*(01), 36-47.

[23] E. G. Christensen, K. T. Lutz, R. J. Spencer, and R. P. Steele, "Persistence of a delocalized radical in larger clusters of hydrated copper(II) hydroxide, $CuOH^{+}(H_2O)_{3-7}$," J. Phys. Chem. A, vol. 127, no. 32, pp. 6647–6659, 2023, doi: 10.1021/acs.jpca.3c03718.

[24] O. Y. Selyutina, P. A. Kononova, V. E. Koshman, L. G. Fedenok, and N. E. Polyakov, "The interplay of ascorbic acid with quinones-chelators—Influence on lipid peroxidation: Insight into anticancer activity," Antioxidants, vol. 11, no. 2, art. no. 376, 2022, doi: 10.3390/antiox11020376.

[25] A. Kola, G. Vigni, M. C. Baratto, and D. Valensin, "A combined NMR and UV–Vis approach to evaluate radical scavenging activity of rosmarinic acid and other polyphenols," Molecules, vol. 28, no. 18, art. no. 6629, 2023, doi: 10.3390/molecules28186629.

[26] B. Brooke, "Artificial intelligence and the emergence of autonomous enterprises: Implications for business model innovation and market dynamics," *Journal of Computational Systems & Engineering Insights*, vol. 4, no. 1, pp. 26–35, 2026.

[27] J.-C. Lavoie and P. Chessex, "Parenteral nutrition and oxidant stress in the newborn: A narrative review," Free Radic. Biol. Med., vol. 142, pp. 155–167, 2019, doi: 10.1016/j.freeradbiomed.2019.02.020.

[28] H. Sun, G. Xie, D. He, and L. Zhang, "Ascorbic acid promoted magnetite Fenton degradation of alachlor: Mechanistic insights and kinetic modeling," Appl. Catal. B: Environ., vol. 267, art. no. 118383, 2020, doi: 10.1016/j.apcatb.2019.118383.

[29] O. Bellamy, "Leveraging entrepreneurial and intrapreneurial orientation to achieve operational excellence in aviation organizations," *International Journal of Business Integrity and Technology Advancements*, vol. 2, no. 1, pp. 20–26, 2026.

[30] T. Moragues, M. Agrachev, S. Mitchell, G. Jeschke, J. Pérez-Ramírez, and A. J. deMello, "Droplet-based EPR spectroscopy for real-time monitoring of liquid-phase catalytic reactions," Small Methods, vol. 9, no. 7, 2025, doi: 10.1002/smtd.202401771.

[31] Y. Zhang, Q. Liu, Q. Lu, Z. Yang, S. Gao, and X. Zhang, "The preparation and dual-mode detection of ascorbic acid based on poly(N-isopropylacrylamide) nanogel with oxidase-like activity," Anal. Methods, vol. 16, no. 26, pp. 4255–4261, 2024, doi: 10.1039/D4AY00638K.

[32] E. M. Ellen, "AI-powered fraud detection: Integrating machine learning, natural language processing, and behavioral analytics for intelligent fraud prevention," *International Journal of Business Integrity and Technology Advancements*, vol. 2, no. 2, pp. 1–7, 2026.

[33] Y. Yuan, J. Mi, and J. Shi, "Smartphone-integrated Ni-HHTP nanozyme sensor for colorimetric detection of ascorbic acid in fresh fruit juices," Phys. Scr., vol. 100, no. 12, art. no. 125011, 2025, doi: 10.1088/1402-4896/ae2549.

[34] L. Hou, Q. Li, J. Li, D. Yang, and Y. Yang, "Cu,Fe,B/Cur-CDs with peroxidase- and ascorbic acid oxidase-like catalytic activity for dual-signal fluorescence sensing of metronidazole," Food Chem., vol. 493, art. no. 145757, 2025, doi: 10.1016/j.foodchem.2025.145757.

[35] I. Alim, R. N. Meghla, T. F. Matin, and T. M. M. H. Prodhan, "A semantic and behavioral AI framework for detecting invoice fraud in automated accounts payable," *International Journal of Science and Research Archive*, vol. 19, no. 2, pp. 1356–1380, 2026.

[36] Martinello F, da Silva EL. Ascorbic acid interference in the measurement of serum biochemical parameters: in vivo and in vitro studies. Clinical biochemistry. 2006 Apr 1;39(4):396-403.

[37] M. Chaudhari, "R2R Plasma-Textured Polymer Films: Nanostructured AR/Hydrophobic Surfaces and EB Cured Varnish Proxies for Scalable Coatings," Genetics and Molecular Research, vol. 25, no. 3, Art. no. 3018, Jul. 27, 2026. doi: 10.4238/e5d1rq05.

[38] Alkhadher SAA, Suratman S, Mohd Sallan MI. An evaluation of spatial and seasonal distributions of dissolved trace metals in the water of the natural wetlands. J Environ Manage. 2023;345:118464. doi:10.1016/j.jenvman.2023.118464

[39] Bottoni C, Tegoni M, Borghesani V. Stability and pseudocatecholase activity of artificial bis-histidyl copper peptides. Inorg Chem. 2025;64(41):20567–76. doi:10.1021/acs.inorgchem.5c02080

[40] M. Chaudhari, "Hydrophilic Nanofiber Barrier Coatings for Aluminum: Waterborne Crosslinking, Microstructure–Property Links, and EIS-Based Protection," Genetics and Molecular Research, vol. 25, no. 3, Art. no. 3017, Jul. 27, 2026. doi: 10.4238/rhd2k915.

[41] Anes B, Bettencourt da Silva RJN, Oliveira C, Camões MF. Seawater pH measurements with a combination glass electrode and high ionic strength TRIS-TRIS HCl reference buffers — an uncertainty evaluation approach. Talanta. 2019;193:118–22. doi:10.1016/j.talanta.2018.09.075

[42] M. A. Jawed, "Uncertainty-aware geostatistical reconstruction of regional groundwater hydraulics under sparse monitoring conditions: A case study of the Evergreen Underground Water Conservation District (EUWCD), Texas, USA," Bishop International Journal of Mathematics and Computer Science, vol. 1, no. 1, pp. 57–71, 2025.

[43] Zhao Y, Zhang H, Jin Q, Jia D, Liu T. Ratiometric optical fiber dissolved oxygen sensor based on fluorescence quenching principle. Sensors. 2022;22(13):4811. doi:10.3390/s22134811

[44] M. A. Jawed, "Comparative analysis of advanced oxidation processes (AOPs) vs. granular activated carbon (GAC) for PFAS removal in US groundwater suppliers: A techno-economic and life cycle

assessment," International Journal of AI, Engineering and Management Studies (IJAIEMS), pp. 72–84, 2025.

[45] Balarak D, Mostafapour FK. Photocatalytic degradation of amoxicillin using UV/synthesized NiO from pharmaceutical wastewater. Indones J Chem. 2019;19(1):211–8. doi:10.22146/ijc.33837

[46] Hassan RM, Ibrahim SM, Khairou KS. Kinetics and mechanism of oxidation of pyruvate by permanganate ion in aqueous perchlorate solution. Transit Met Chem. 2018;43(8):683–91. doi:10.1007/s11243-018-0257-x

[47] Miller JN, Miller JC. Statistics and chemometrics for analytical chemistry. 7th ed. Harlow: Pearson Education; 2018.